JSS Focus Issue on Visible and Infrared Phosphor Research and Applications

Microscopic Study of Dopant Distribution in Europium Doped $SrGa_2S_4$: Impact on Thermal Quenching and Phosphor Performance

Lisa I. D. J. Martin,[a,b] Dirk Poelman,[a,b,*] Philippe F. Smet,[a,b,*,z] and Jonas J. Joos[a,b,z]

[a]*Department of Solid State Sciences, LumiLab, Ghent University, Ghent, Belgium*
[b]*Center for Nano- and Biophotonics, Ghent University, Ghent, Belgium*

White light emitting diodes start to dominate lighting and display applications. However, the properties of the phosphors used in these devices strongly depend on synthesis conditions. A better understanding of how performance-determining mechanisms such as thermal quenching are influenced by synthesis conditions and sample composition is necessary to achieve the required standards in a goal-oriented strategy. In this paper, a microscopic thermal quenching study on green-emitting $SrGa_2S_4:Eu^{2+}$ phosphors by means of cathodoluminescence spectroscopy and energy dispersive X-ray analysis in a scanning electron microscope is used to extend our knowledge beyond averaged information obtained on bulk material. Elemental and cathodoluminescence mapping at different temperatures made it possible to determine thermal quenching profiles for sub-micrometer sized areas. These revealed a broad range of local quenching temperatures for samples with ill-distributed dopant ions. For the associated activation energy an upper limit of 0.61 eV was identified, corresponding to the intrinsic thermal quenching of isolated europium ions. Furthermore, the results confirm a previously suggested thermal quenching model which involves the presence of both isolated and clustered dopant ions.
 [DOI: 10.1149/2.0341709jss]

Manuscript submitted August 14, 2017; revised manuscript received September 6, 2017. Published September 15, 2017. *This paper is part of the JSS Focus Issue on Visible and Infrared Phosphor Research and Applications.*

Inorganic luminescent materials or phosphors are currently applied on a large scale in various novel technologies. Most notably, white light-emitting diodes (LEDs), which are applied in lighting and display technologies, rely on high-performance phosphors.[1–3] Here, the emission of a blue light source, based on a $Ga_{1-x}In_xN$ LED chip is partly absorbed by the phosphor blend that is applied on top of this chip or in a remote fashion.[4–6] The phosphor re-emits the absorbed energy as green, yellow and red light, which is mixed with the remaining blue LED emission as to get an overall white emission. This requires subtle fine-tuning, both in terms of material composition,[7,8] as well as device manufacturing[5,9] to achieve white LED devices with the desired properties.

From the materials point of view, phosphor properties are highly dependent on synthesis conditions, often in an unpredictable and hard-to-control way. This can be attributed to an incomplete understanding of the underlying physical mechanisms for various macroscopic properties.[10] As an example, thermal quenching (TQ), i.e. the decreased internal quantum efficiency of luminescent materials at elevated temperatures, has been attributed to various causes, either intrinsic to the luminescent center itself or due to external influences such as the presence of defects or the local clustering of luminescent ions.[10,11] The undetermined nature of TQ makes it difficult to engineer synthesis routines to yield phosphors with a minimized TQ and an optimized performance.

Phosphors are generally studied at the macroscopic level, i.e measurements are typically performed on milligram quantities, a scale which is of relevance for applications. Nonetheless, if materials are inhomogeneous in terms of structure or chemical composition, the local physical properties of the material can show differences on a microscopic scale. When performing a macroscopic characterization of the luminescent properties, all local contributions are averaged out, and no detailed information on the interplay between structure and luminescence can be obtained.

Cathodoluminescence (CL) spectroscopy in a scanning electron microscope (SEM) can overcome this limitation by allowing to study emission characteristics at the microscopic scale.[12–14] When combining CL with an energy-dispersive X-ray (EDX) detector, one also obtains the local distribution of the elements present, which would not be available via optical microscopy. In SEM-CL-EDX, simultaneous identification of the morphology, the chemical composition and the spectral distribution of a phosphor with a spatial resolution down to 1 μm or less is achieved. When using a fast beam blanker, local decay time analysis and spectrally resolved decay time mapping can be performed.[15,16] A temperature stage allows to evaluate thermal quenching at the sub-micron scale.[17] The correlation of the local compositional and luminescent properties has the potential to lead to a more profound understanding of the behavior of a phosphor and luminescence mechanisms in general. This technique has been successfully applied to study local compositional differences,[17–20] dopant clustering,[21] impurity phases[22,23] and particle size inhomogeneity[21,24,25] in phosphors. Single particle studies thus increase our knowledge on phosphor properties and often lead to the discovery of interesting novel phenomena.[26–28]

In this work we apply SEM-CL-EDX to study the thermal quenching behavior of europium doped strontium thiogallate, $SrGa_2S_4:Eu^{2+}$. This material is known as a saturated green phosphor, especially suitable for display applications.[9,29–33] It was deduced from macroscopic TQ and luminescence decay measurements that two types of Eu ions determine the luminescent properties, i.e. isolated Eu ions, showing a textbook-like behavior and Eu clusters, responsible for accelerated thermal quenching.[33] It is our aim to validate this simple model by a microscopic study of the thermal quenching behavior.

Materials and Methods

Preparation of $SrGa_2S_4:Eu^{2+}$.—$SrGa_2S_4:Eu^{2+}$ powders were prepared in a single-step solid state synthesis where stoichiometric amounts of SrS (Alfa Aesar, 99.9%), Ga_2S_3 (Alfa Aesar, 99.99%) and EuF_3 (Alfa Aesar, 99.5%) were mixed and subsequently heat treated in an atmosphere of forming gas (90% N_2, 10% H_2 mixture), inside alumina crucibles. The samples were heated for two hours at a rate of 7.5°C/min and kept at 900°C for another two hours. After that, they were allowed to cool naturally and were slightly ground. The samples looked homogeneous upon visual inspection both under daylight and UV light.

The phase purity of all the prepared powders was validated using X-ray diffraction (XRD), utilizing $CuK\alpha_1$ radiation on a Siemens D5000 diffractometer (40 kV, 40 mA) before further investigation.

*Electrochemical Society Member.
[z]E-mail: Philippe.Smet@ugent.be; Jonas.Joos@ugent.be

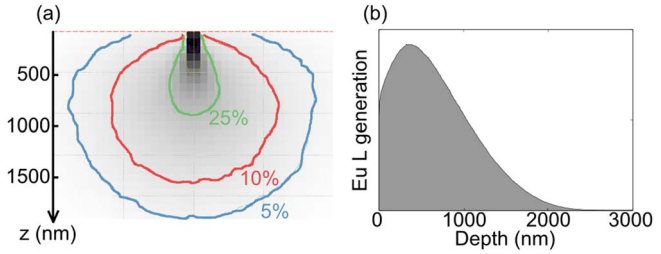

Figure 1. (a) Electron energy relative to the incident beam energy and (b) origin of the detected Eu L_α X-rays in $SrGa_2S_4:Eu^{2+}$ according to the used electron beam settings. Both images were obtained through a Monte Carlo simulation of electron trajectories with the software Casino.[4]

Photoluminescence quantum efficiencies were obtained upon LED excitation of the powder inside an integrating sphere (LabSphere, GPS-SL series, 152 mm diameter, Spectralon coated). Al_2O_3 was used as a white reflecting standard.

Cathodoluminescence and energy dispersive X-ray spectroscopy in a scanning electron microscope.—Scanning electron microscopy was performed in a Hitachi S-3400 N, equipped with a ThermoScientific Noran System 7 for energy-dispersive X-ray analysis. Cathodoluminescence was captured with an optical fiber attached to an Acton SP2300 monochromator and ProEM 1600 EMCCD camera, both from Princeton Instruments, which allows spectrally resolved CL mappings. Furthermore, a Deben heating and cooling stage with Peltier element was assembled in the SEM, such that the sample temperature could be controlled between 250 K and 400 K. All measurements were performed at a pressure of 25 Pa in order to avoid sample charging, with an accelerating voltage of 20 kV. The characteristic X-ray lines for Sr (L_α, 1.8 keV), Ga (K_α, 9.2 keV), S (K_α, 2.3 keV) and Eu (L_α, 5.8 keV) were used for elemental mapping. EDX and CL spectra were collected simultaneously with a dwell time of 100 ms per pixel in a 256-by-184 grid.

From Figure 1 it can be deduced that the majority of CL (Fig. 1a) and EDX Eu L_α signals (Fig. 1b) in $SrGa_2S_4:Eu^{2+}$ will arise from the same region in the studied sample, i.e. 0 to 1 μm beneath the surface. Therefore it is allowed to correlate both results, as will be done in this paper. Furthermore, dopant concentrations were determined via the ratio of the Eu L_α signal to the Ga K_α signal, in order to avoid using low energy Sr $L_\alpha$and S K_α X-rays which are prone to shadow effects.

Results and Discussion

Dopant distribution.—Figure 2 shows microscopic images of $Sr_{0.97}Ga_2S_4:Eu_{0.03}$, prepared by a solid state synthesis, collected at two different magnifications in Figs. 2a and 2c. This allows to appreciate sample inhomogeneity on the *single grain* level (in the 0.1 μm range) as well as on a larger scale, considering multiple grains (in the 5–20 μm range). As can be seen in Fig. 2c, the examined area is actually a conglomerate of several single particles. In this text this will be referred to as a single grain, in order to differentiate from the multi-grain level. For both situations, an elemental mapping by means of EDX was performed and the result for Eu is shown in Figs. 2b and 2d. As depicted in the figure, the dopant ions are not uniformly distributed over the phosphor, leading to substantial local variations. No significant variations in the concentrations of the other elements (Sr, Ga, S) were observed (not shown).

Not only over various grains, but even within a single grain the Eu concentration shows a broad distribution. As can be seen in Fig. 2d the Eu ions tend to cluster, which can lead to elevated local Eu concentrations. This implies that other areas will contain a lower amount of Eu than intended.

This non-uniform distribution of europium can be ascribed to an incomplete diffusion process during the solid state synthesis. Possible improvements could be an extension of the heat-treatment, using a more reactive H_2S atmosphere instead of forming gas or relying on a more thorough mixing of the precursor materials, e.g. by automated ballmilling or working with a co-precipitation step. These improvements are not immediately pursued here as our main goal is to correlate the thermal quenching behavior of the Eu^{2+} luminescence to the local dopant concentration.

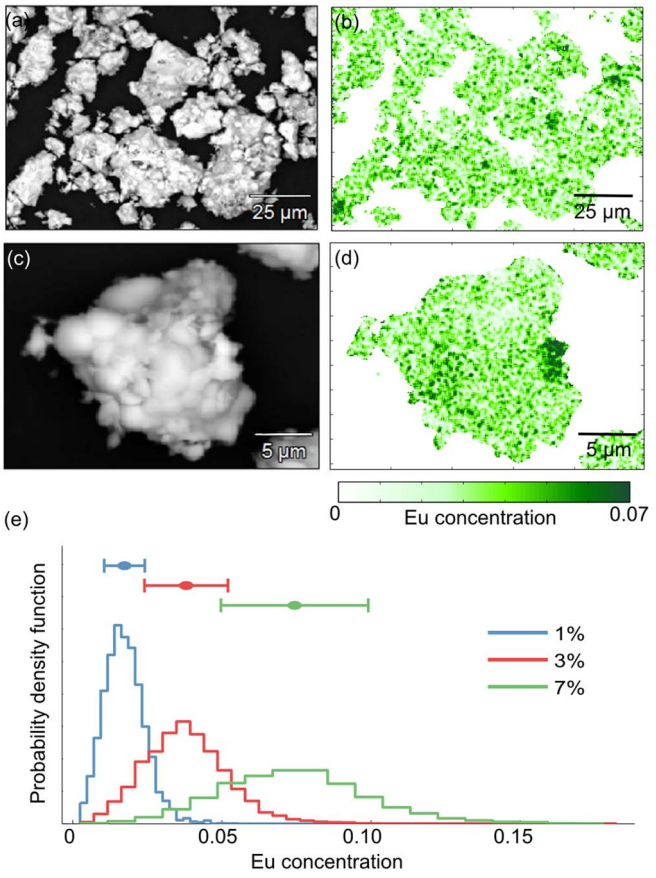

Figure 2. Backscattered electron image and local molar Eu concentration from EDX for $Sr_{0.97}Ga_2S_4:Eu_{0.03}$ for (a-b) multiple grains and (c-d) a single grain. (e) Spread on the local Eu concentration over several grains for $Sr_{1-x}Ga_2S_4:Eu_x$ with $x = 0.01$, 0.03 and 0.07, measured over a total area of 90 μm by 130 μm.

Fig. 2e shows the distribution of the local Eu concentration over several grains for three different powders with nominal europium concentrations of 1%, 3% and 7%. As they were collected for multiple grains, these broad distributions can be considered as the superposition of the distributions of the individual grains, all having their unique average and width in the case of this inhomogeneous powder. When comparing the three measurements, one finds that the variation of local dopant concentration, i.e. the width of the distribution, becomes larger when the introduced dopant amount increases. For higher doping concentrations, it is hence more likely to reach a situation where the dopant is widely distributed. It is also important to note that on average, the measured samples do contain the intended amount of Eu. The average Eu concentrations for the measured multi-grain areas are $1.5 \pm 0.75\%$, $3.2 \pm 1.3\%$ and $7.2 \pm 2.9\%$, meaning that all samples have an equally ill-distributed amount of dopant.

The chemical inhomogeneity of the prepared powders will result in a similar inhomogeneity in physical properties such as emission spectrum, photoluminescence quantum efficiency (QE) and TQ. Measurement of the bulk absorption spectrum reveals about 30% of absorption over a wide range of wavelengths as described in.[33] This is presumably due to the presence of intrinsic defects. A large fraction of the absorbed energy does hence not reach the Eu^{2+} ions and results in

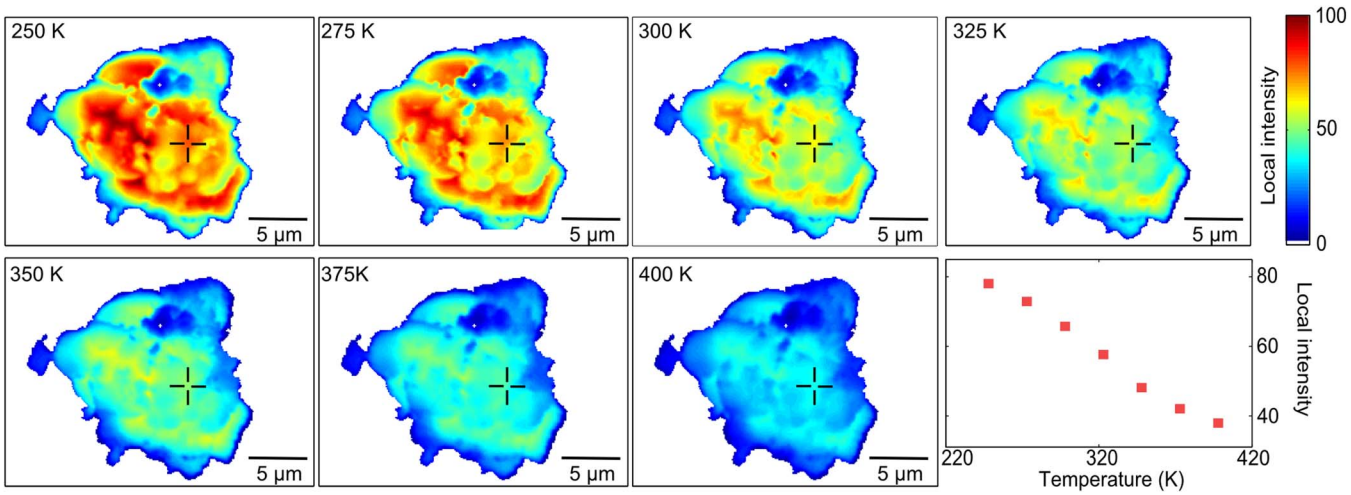

Figure 3. CL intensity maps for the single phosphor grain, as shown in Fig. 2c–2d, measured at different temperatures. The local thermal quenching profile (bottom, right) was constructed from the CL intensity in the region of interest, indicated by the cross hairs in the CL maps. CL emission was captured using an optical fiber positioned at the right of the studied area.

a relatively low quantum efficiency of around 45% in this case. The presence of intrinsic defects can additionally cause an early onset of the TQ when these are able to interact with the excited Eu^{2+} ions. This is investigated in the following sections.

Effect on TQ.—Bulk measurements have shown that increasing the dopant concentration lowers the performance of phosphors at elevated temperatures.[34] Therefore it is reasonable to assume that a non-uniform dopant distribution will have its influence on the thermal quenching behavior. In this section the extent of this influence is studied by means of SEM-CL-EDX mappings of the same region of interest, at a range of temperatures. After calculating the local intensity changes as a function of temperature, the local thermal quenching behavior and the effective local dopant concentration can be correlated, offering a unique microscopic view on thermal quenching.

Processing of TQ maps.—The studied area was divided into 256-by-184 'pixels' of about 0.10 µm by 0.10 µm. During the scanning an EDX as well as a CL spectrum was obtained for each pixel. Afterwards, the CL spectrum was processed to determine local emission properties such as total intensity. To compare the maps measured at seven different temperatures (from 250 K to 400 K, every 25 K), it was important to make sure they spatially coincided. However, because of electrostatic charging and the change in temperature the images can be distorted. A careful alignment procedure was thus performed to avoid artefacts.[17] As shown in Fig. 3, the resulting intensity maps then allowed to generate a thermal quenching profile for each relevant pixel of the studied area.

In order to facilitate the data interpretation, all obtained thermal quenching profiles – both at the single pixel level as for the average behavior - were fitted by means of a standard single-barrier model, a widely used prescription to model thermal quenching behavior:[35–37]

$$I(T) = \frac{I(0)}{1 + A \exp\left(\frac{-\Delta E_T}{k_B T}\right)} \qquad [1]$$

where $I(T)$ stands for the intensity at temperature T and k_B is the Boltzmann constant.

Next to the barrier height or activation energy ΔE_T, this fitting procedure yields an estimate of $T_{0.5}$, i.e the temperature for which the emission intensity drops to half of the value at low temperature, for every submicrometer-sized area. $T_{0.5}$ is a parameter which is typically used to quantify the bulk performance of a phosphor.[3] In this equation, A is given by the ratio of the radiative and non-radiative decay rates of the excited state governing the luminescence. Despite the careful alignment of the CL maps for different temperatures, some pixel groups can still suffer from a bad alignment. To filter these out of the post-analysis, only those fits with an R^2 value of 0.985 or higher were taken into account. This corresponds with 75% to 90% of the studied pixels, demonstrating both the quality of the alignment procedure and the suitability of Eq. 1 to describe thermal quenching behavior.

Results for $SrGa_2S_4:Eu^{2\pm}$.—The local thermal quenching behavior was studied for $Sr_{1-x}Ga_2S_4:Eu_x$ phosphors with $x = 0.01$, 0.03 and 0.07.

The results presented in this section were obtained by mapping single grains. Since the dopant distribution for these samples varies a lot from one grain to another, the outcome of these single grain measurements may not be generalized for the entire phosphor. Nevertheless, they do give a good idea of the heterogeneity of phosphor properties at the local scale.

Figure 4a shows several of the fits according to Eq. 1 that were performed per pixel on a single grain mapping of the 3% doped sample, which was also shown in Figs. 2c–2d. In the left figure, it can be seen that the various TQ curves within the single grain vary over a broad range of about 75 K. The bold line indicates the overall thermal behavior of the studied phosphor grain, which was established by integrating over all pixels, similar to what happens during bulk TQ

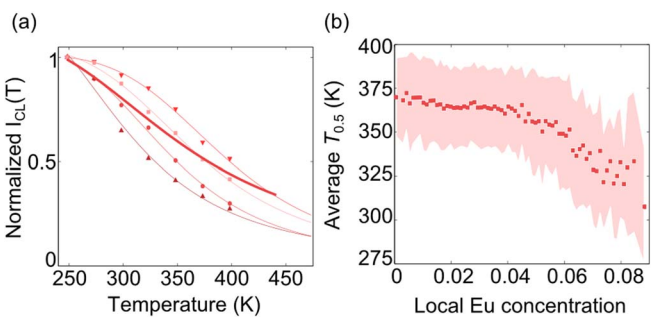

Figure 4. (a) Examples of local TQ profiles (with markers) compared to the averaged TQ behavior (bold line) of the $Sr_{0.97}Ga_2S_4:Eu_{0.03}$ grain shown in Figs 2c–2d and 3. (b) Resulting $T_{0.5}$ (in K) averaged per local Eu concentration (markers) and corresponding standard deviation (shaded area).

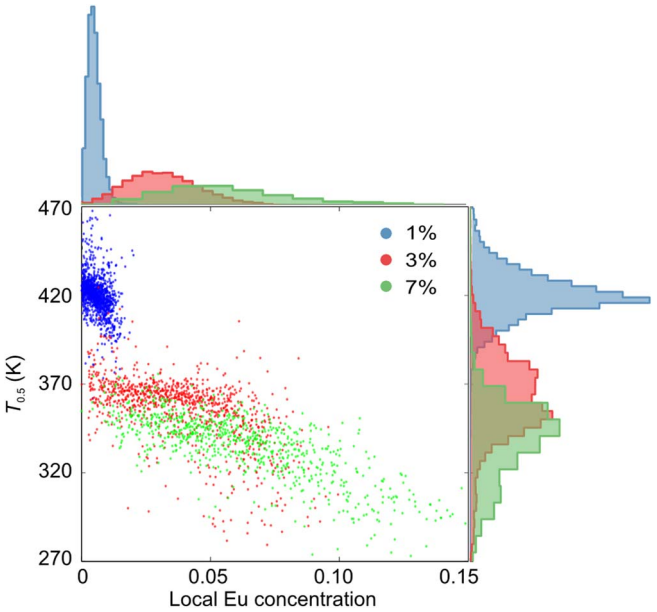

Figure 5. Distribution of local Eu concentration related to the distribution of local $T_{0.5}$ within a single phosphor grain for $Sr_{1-x}Ga_2S_4:Eu_x$ with $x = 0.01$, 0.03 (shown in Figs. 2c–2d and 3) and 0.07.

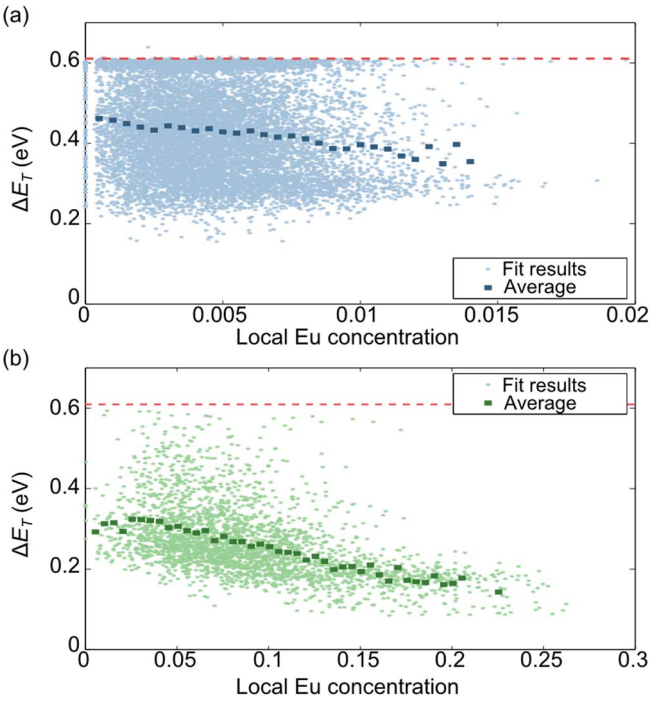

Figure 6. Fit results for ΔE_T (in eV) as a function of local Eu concentration for $Sr_{1-x}Ga_2S_4:Eu_x$ with (a) $x = 0.01$ and (b) $x = 0.07$. The red dotted line indicates the maximum value of 0.61 eV that was found for ΔE_T.

measurements. Because of the large variation of local TQ curves, it is possible that the sum of all those contributions appears to behave different to Eq. 1, making it impossible to simply fit the average behavior with the standard equation. By taking the sum of all these very different local components, the slope of the overall TQ curve will be lower than expected. Therefore, the slope of bulk TQ plots is far more representative for the quality of the synthesis than the average $T_{0.5}$ value, since the former can be related to the local dopant distribution.

The procedure outlined in Fig. 4a is then performed for all pixels with sufficiently high emission intensity, such that a $T_{0.5}$ value can be assigned to every pixel. This mapping of the TQ is then available for further processing and correlation to other data sets, such as the dopant concentration measured by EDX.

Figure 4b confirms the connection between $T_{0.5}$ and local Eu concentration. To construct this figure, the $T_{0.5}$ values were averaged for all pixels having a certain Eu concentration. The shaded area demonstrates the standard deviation on these results. From the figure, it is clear that a larger dopant amount coincides with a lower quenching temperature, such that dopant clustering hampers the thermal performance of the phosphor. The image in Fig. 4b gives a unique view on the microscopic phenomenon of concentration quenching where the excitation energy can travel over substantial distances in the phosphor by energy transfer between nearby europium ions. If one of these europium ions is next to a luminescence killer center, this offers a fast route for non-radiative dissipation.

Figure 5 shows the spread on local Eu concentration and corresponding $T_{0.5}$ within a single grain for each of the three studied samples. It is again observed that a higher Eu concentration corresponds to a lower $T_{0.5}$. For lightly doped $SrGa_2S_4:Eu^{2+}$ the variation on $T_{0.5}$ is significantly less than for the other samples, in correspondence with its narrower Eu distribution. For ill-distributed Eu ions, which is often the case when introducing high doping concentrations, the local variation on $T_{0.5}$ becomes larger. Moreover, these distributions are shifted toward lower $T_{0.5}$, due to the presence of dopant clusters with reduced thermal performance. Therefore the quality of the dopant distribution not only affects the spread on $T_{0.5}$ but also its average value. Limiting dopant concentrations ensures more homogeneous phosphor properties throughout the sample, simply because the possibility for excessively heavy doped regions is smaller.

The followed fitting approach does not only yield the characteristic temperature $T_{0.5}$, but additionally allows to obtain the distribution of the associated energy barrier height, ΔE_T, a parameter which is often considered as being a direct measure for the underlying electronic structure of the luminescent ion. Along with the non-radiative decay rate and the overlap of vibrational wavefunctions of initial and final states, it determines the thermal quenching profile.[38] A reliable determination of the parameter ΔE_T is hence an important empirical input in the quest to explain the mechanism behind thermal quenching. As for the quenching temperature, important local variations are however expected and bulk measurements are deemed to provide only an average ΔE_T value.

Figure 6 shows the distribution of ΔE_T from two CL maps, corresponding respectively to a single grain with low Eu concentration (Fig. 6a) and a single grain with a higher doping concentration (Fig. 6b). It is clear from the figure that an upper limit exists, corresponding to a ΔE_T value of 0.61 eV. This upper limit is more regularly met throughout the lightly doped sample (Fig. 6a), predominantly for lower local Eu concentrations. For the heavily doped sample (Fig. 6b) only a small number of scanned areas reaches this maximal energy barrier height, clearly related to the absence of areas with very low dopant concentration.

From these results, it seems plausible to assume that this value of $\Delta E_T = 0.61$ eV corresponds to the *ideal situation* of an Eu ion which is sufficiently isolated to avoid interaction with neighboring Eu ions or other defects that generate non-radiative decay paths, leading to an optimal thermal performance. The analysis reveals that the majority of the Eu ions displays a lower ΔE_T, suggesting that the energy barrier is lowered because of energy transfer possibilities or the presence of other non-radiative decay paths. This confirms the proposition in[22] that two types of Eu sites are present in the phosphor: isolated ions and ions surrounded by other dopant ions, allowing energy transfer and a higher probability for non-radiative decay. Nonetheless, even for the lowest local Eu concentrations, only a limited fraction of the pixels give rise to this maximal activation energy. This indicates that even when the Eu ions are isolated, a stronger TQ can be found, most likely due to the presence of intrinsic defects, as was already suggested by the QE

measurement. Irrespective of this finding, the clear emergence of the optimal activation energy value proves the validity of our technique to identify the intrinsic thermal quenching and hence to disclose the fundamental limitations of phosphor materials, even for not yet fully optimized syntheses. The value of 0.61 eV obtained in this work for $SrGa_2S_4:Eu^{2+}$ is close to the value of 0.6 eV that was obtained from bulk measurements by Chartier et al., which is not surprising given the low doping concentration of 0.1% that was used.[29]

The proposed microscopic technique allows to extract the thermal quenching energy barrier for an *ideally* incorporated dopant ion instead of an average value obtained from a bulk measurement, unavoidably having contributions from *non-ideal* luminescent centers. The optimal ΔE_T value is hence well suited for direct comparison with electronic structures determined empirically or from first principles. In the case of Eu^{2+} $4f^65d\text{-}4f^7$ emission, commonly used models assume that thermal quenching proceeds via the brief creation of an exciton or an europium trapped exciton.[36,39–41] This is usually quantified from empirical band diagrams where the distance between the 5d level of the Eu^{2+} impurity and the host conduction band is identified with ΔE_T. Two such band diagrams can be found in literature for $SrGa_2S_4$:Eu, yielding values of 0.43 eV and 0.97 eV.[42,43] These values are prone to large uncertainties of 0.3–0.4 eV.[37] Due to the large uncertainties on calculated energy differences and the large density of excited states in the relevant energy range, it still remains almost impossible to reliably pinpoint which states contribute to phenomena such as thermal quenching. There is hence an ongoing need for more accurate models as well as reliable experimental data, corresponding to optimized systems. It is clear that temperature-dependent CL spectroscopy can contribute to the latter, allowing to reveal idealized behavior, even in the case where the synthesis of the materials has not yet been optimized or where larger dopant concentrations are used in order to meet with the technological requirements.

Conclusions

Temperature dependent SEM-CL-EDX mappings were performed to study the local thermal quenching behavior of $SrGa_2S_4:Eu^{2+}$. The dopant distributions of the studied samples revealed considerable differences between individual phosphor grains, as well as within a single grain. For non-optimized syntheses, the dopant is not homogeneously spread over the sample and tends to cluster. Since bulk phosphor properties are known to depend on the doping concentration, the thermal quenching behavior was studied on a sub-micrometer scale and compared to the local Eu concentration.

It was found that a higher dopant concentration reduces thermal performance, thus resulting in a lower quenching temperature $T_{0.5}$. In case of an imperfect dopant distribution in the sample, a considerable spread is additionally found on $T_{0.5}$. Consequently this parameter is inadequate as the sole representative for the thermal performance of a phosphor. When a bulk thermal quenching curve does not follow the standard single-barrier model however, this can be an indication for a large variation in local TQ behavior, possibly due to a heterogeneous dopant distribution. Therefore the shape of bulk TQ plots is important to assess the quality of the synthesis, next to the standard-reported bulk $T_{0.5}$ value.

When the dopant ions are well-distributed over the sample, the majority of luminescent centers will be isolated and behaves according to the *ideal* situation, guaranteeing optimum thermal performance. In the case of $SrGa_2S_4:Eu^{2+}$, this was characterized by a well-defined maximal value of 0.61 eV for the activation energy of the single-barrier model. A distribution of lower-lying activation energies were found, representing luminescent centers that are more prone to non-radiative decay channels. This case study showed that a microscopic investigation can yield a deeper insight into the various processes that determine the performance of luminescent materials, contributing to a more profound understanding of the underlying mechanisms as well as how these materials can be optimized for the intended application.

Acknowledgments

DP, PFS and JJJ thank the IWT-Vlaanderen for the SBO-IWT grant LumiCoR (SBO130030). Olivier Janssens is acknowledged for his assistance with the numerous XRD measurements.

References

1. E. F. Schubert, J. K. Kim, H. Luo, and J. Q. Xi, *Rep Prog Phys*, **69**(12), 3069 (2006).
2. H. A. Hoppe, *Angew. Chem. Int. Edit.*, **48**(20), 3572 (2009).
3. P. F. Smet, A. B. Parmentier, and D. Poelman, *J. Electrochem. Soc.*, **158**(6), R37 (2011).
4. B. C. Li, N. Z. Zhuo, W. Q. Li, Q. Y. He, R. X. Huang, G. X. Liu, E. G. Ye, and H. B. Wang, *Spectrosc Spect Anal*, **37**(3), 728 (2017).
5. J. Ryckaert, S. Leyre, P. Hanselaer, and Y. Meuret, *Opt. Express*, **23**(24), A1629 (2015).
6. S. H. Abdullayeva, T. Y. Orujov, N. N. Musayeva, R. B. Jabbarov, and S. K. Orujov, *World Journal of Nano Science and Engineering*, **7**, 17 (2017).
7. V. Bachmann, C. Ronda, O. Oeckler, W. Schnick, and A. Meijerink, *Chem. Mater.*, **21**(2), 316 (2009).
8. Z. Xia and A. Meijerink, *Chem Soc Rev*, **46**(1), 275 (2017).
9. S. Abe, J. J. Joos, L. I. D. J. Martin, Z. Hens, and P. F. Smet, *Light-Sci Appl*, **6**, e16271 (2017).
10. P. F. Smet and J. J. Joos, *Nat Mater*, **16**(5), 500 (2017).
11. J. Ueda, A. Meijerink, P. Dorenbos, A. J. J. Bos, and S. Tanabe, *Phys Rev B*, **95**(1), 014303 (2017).
12. D. den Engelsen, G. R. Fern, P. G. Harris, T. G. Ireland, and J. Silver, *Materials*, **10**(3), 312 (2017).
13. M. R. Phillips, *Microchim Acta*, **155**(1–2), 51 (2006).
14. Y. Cho, B. Dierre, T. Sekiguchi, T. Suehiro, K. Takahashi, T. Takeda, R. J. Xie, Y. Yamamoto, and N. Hirosaki, *Jove-J Vis Exp*, (117), e54249 (2016).
15. D. Poelman and P. F. Smet, *Physica B*, **439**, 35 (2014).
16. B. G. Yacobi and D. B. Holt, *J. Appl. Phys.*, **59**(4), R1 (1986).
17. P. F. Smet, J. Botterman, A. B. Parmentier, and D. Poelman, *Opt. Mater.*, **35**(11), 1970 (2013).
18. B. Dierre, X. L. Yuan, K. Inoue, N. Hirosaki, R.-J. Xie, and T. Sekiguchi, *J Am Ceram Soc*, **92**(6), 1272 (2009).
19. A. B. Parmentier, P. F. Smet, F. Bertram, J. Christen, and D. Poelman, *J. Phys. D - Appl. Phys.*, **43**(8), 085401 (2010).
20. J. J. Joos, K. Korthout, S. Nikitenko, D. Poelman, and P. F. Smet, *Opt. Mater. Express*, **3**(9), 1338 (2013).
21. R. P. S. Chakradhar, B. J. Basu, and R. V. Lakshmi, *Spectrochimica Acta Part A: Molecular and Biomolecular Spectroscopy*, **78**(2), 783 (2011).
22. A. V. Vishnyakov, E. A. Vishnyakova, T. Y. Kiseleva, and I. V. Ivanov, *Mendeleev Communications*, **25**(4), 299 (2015).
23. K. Takahashi, B. Dierre, Y. J. Cho, T. Sekiguchi, R. J. Xie, and N. Hirosaki, *J Am Ceram Soc*, **98**(4), 1253 (2015).
24. J. Adam, W. Metzger, M. Koch, P. Rogin, T. Coenen, J. S. Atchison, and P. Konig, *Nanomaterials-Basel*, **7**(2), 26 (2017).
25. B. Dierre, X. Yuan, and T. Sekiguchi, *Sci Technol Adv Mat*, **11**(4), 043001 (2010).
26. N. Hirosaki, T. Takeda, S. Funahashi, and R.-J. Xie, *Chem. Mater.*, **26**(14), 4280 (2014).
27. X.-J. Wang, S. Funahashi, T. Takeda, T. Suehiro, N. Hirosaki, and R.-J. Xie, *J Mater Chem C*, **4**(42), 9968 (2016).
28. X.-J. Wang, L. Wang, T. Takeda, S. Funahashi, T. Suehiro, N. Hirosaki, and R.-J. Xie, *Chem. Mater.*, **27**(22), 7689 (2015).
29. C. Chartier, C. Barthou, P. Benalloul, and J. M. Frigerio, *J. Lumin.*, **111**(3), 147 (2005).
30. C. Chartier, P. Benalloul, C. Barthou, J. M. Frigerio, G. O. Mueller, R. Mueller-Mach, and T. Trottier, *J. Phys. D - Appl. Phys.*, **35**(4), 363 (2002).
31. C. Hidaka and T. Takizawa, *J. Phys. Chem. Solids*, **69**(2–3), 358 (2008).
32. M. Nazarov, D. Y. Noh, and H. Kim, *Mater Chem Phys*, **107**(2–3), 456 (2008).
33. J. J. Joos, K. W. Meert, A. B. Parmentier, D. Poelman, and P. F. Smet, *Opt. Mater.*, **34**(11), 1902 (2012).
34. V. Bachmann, C. Ronda, and A. Meijerink, *Chem. Mater.*, **21**(10), 2077 (2009).
35. N. F. Mott, *Proceedings of the Royal Society of London. Series A. Mathematical and Physical Sciences*, **167**(930), 384 (1938).
36. P. Dorenbos, *J. Phys.-Condens. Mat.*, **17**(50), 8103 (2005).
37. J. J. Joos, D. Poelman, and P. F. Smet, *Phys. Chem. Chem. Phys.*, **17**(29), 19058 (2015).
38. C. W. Struck and W. H. Fonger, *Understanding Luminescence Spectra and Efficiency Using Wp and Related Functions*, 2012: Springer Berlin Heidelberg.
39. G. Blasse, W. Schipper, and J. J. Hamelink, *Inorg Chim Acta*, **189**(1), 77 (1991).
40. M. Ando and Y. A. Ono, *J Cryst Growth*, **117**(1–4), 969 (1992).
41. U. Happek, S. A. Basun, J. Choi, J. K. Krebs, and M. Raukas, *J Alloy Compd*, **303**, 198 (2000).
42. J. J. Joos, D. Poelman, and P. F. Smet, *Opt. Mater.*, **61**, 50 (2016).
43. A. Dobrowolska, B. Dierre, C. M. Fang, H. T. Hintzen, and P. Dorenbos, *J. Lumin.*, **184**, 256 (2017).